

# Accuracy Evaluation of Different Centerline Approximations of Blood Vessels

A. La Cruz

Institute of Computer Graphics and Algorithms, Vienna University of Technology

---

## Abstract

*Accurate determination of the central vessel axis is a prerequisite for automated arteries diseases visualization and quantification. In this paper we present an evaluation of different methods used to approximate the centerline of the vessel in a phantom simulating the peripheral arteries. Six algorithms were used to determine the centerline of a synthetic peripheral arterial vessel. They are based on: ray casting technique using thresholds and maximum gradient-like stop criterion, pixel motion estimation between successive images called block matching, center of gravity and shape based segmentation. The Randomized Hough Transform and ellipse fitting using Lagrange Multiplier have been used as shape based segmentation techniques, fitting an elliptical shape to a set of points. The synthetic data simulate the peripheral arterial tree (aorta-to-pedal). The vessel diameter changes along the z-axis from about 0.7 to about 23 voxels. The data dimension is 256x256x768 with voxel size 0.5x0.5x0.5mm. In this data set the centerline is known and an estimation of the error is calculated in order to determine how precise a given method is and to classify it accordingly.*

Categories and Subject Descriptors (according to ACM CCS): I.3.3 [Blood Vessel]: Centerline detection, Vessel segmentation, Medical Visualization

---

## 1. Introduction

Peripheral arterial occlusive disease (PAOD) is a manifestation of arteriosclerosis. Epidemiological and clinical studies have shown that PAOD increases the risk of cardiovascular and cerebrovascular events and mortality [PGJ03]. CT-angiography (CTA) has evolved into a routinely applicable non-invasive vascular imaging technique for many vascular territories such as the peripheral (lower extremity) arteries. Accurate identification of the vessel centerline in CTA data sets is highly desirable, because of its central role in vessel visualization (e.g., through curved planar reformations - CPR [KFW\*02]) and automated vessel analysis and quantification.

The vessel centerline is widely used for 3D reconstruction and modelling of vessel structures. It has been used as base of several vessel segmentation techniques [KQ00] and as starting point for a geometric model definition of vascular structures [BFC03].

As a general approach, the skeletonization of a vascular structure is a method widely used for centerline detection [Pui98b, Pui98a]. Several methods based on the skele-

tonization approach use thresholding and object connectivity [NKSK93], distance field calculation [PTN97], mathematic morphology or a thinning process based on dilation, erosion, opening and closing operators [TKN\*95]. These approaches have been applied in different image modalities and vascular structures. Many of them have been applied on a specific image modality (e.g., MRI and/or CTA) or in a specific part of the vessel structure, for examples, cerebrovascular structures [Pui98b] or coronary arteries from biplane angiograms [KTS88, CRC92] or aorta [WNV00]. Nevertheless these techniques and methods have not been applied to the centerline detection of tubular structures on peripheral vessels, where the level of intensity decreases from top to bottom, from aorta to pedal (tibial and fibular arteries). On peripheral arteries result difficult an accuracy detection of the centerline, where the diameter can be between 2 to 4 voxels. The partial volume effect makes also correct identification of small vessels (e.g. tibial and fibular arteries) difficult.

In this work, we present the results of an accuracy evaluation of six techniques used to approximate the vessel cen-

terline in peripheral arteries. A synthetic data set where the diameter varies from about 0.7 to about 23 voxels is used in order to evaluate the accuracy of different methods. The results are compared and evaluated. This paper has the following structure. In section 2 we describe each method we have evaluated. In section 3 we present the evaluation and results of the different methods applied. Finally in section 4 we present the conclusions and future work.

## 2. Centerline Approximation Methods

Starting from an initial path of the vessel, six different techniques to approximate the vessel centerline were applied in order to evaluate accuracy and quality. This initial path is calculated using the vessel tracking technique developed by Kanitsar [KWF\*01].

The vessel tracking method is used in order to find a path with high probability inside the vessel structure. This technique is based on Dijkstra's algorithm [Dij59], which is used to find the shortest path from a single source vertex or node to all other vertices in a weighted, directed graph. Initially, the user interactively marks a start and end point. These two seed points must be selected inside the vessel and indicate a vessel segment. Each voxel is considered a vertex or a node in a directed graph structure, and the connection with any of its adjacent voxels as edges. Each edge has an associated weight defined by the following cost function:

$$f_C(x, y) = c_{step} + f_I(y) + f_G(x, y) + f_L(y) \quad (1)$$

Eq. 1 defines a local cost function between a voxel  $x$  and its adjacent voxel  $y$ . The constant  $c_{step}$  keeps the curvature of the path inside the vessel low. The function  $f_I(y)$  assigns low penalty to voxels whose density values are inside the density interval defined for a vessel (see Fig. 1), and high penalty in other case. In Eq. 2, 3, and 4,  $f(y)$  is the density value for the voxel  $y$ . The values  $c_{lowerBorder}$ ,  $c_{lower}$ ,  $c_{upper}$ , and  $c_{upperBorder}$  are used like thresholds to identify a vessel from other tissues. Density values in the interval defined by  $c_{lowerBorder}$  and  $c_{upperBorder}$  are considered density values for vessels. Furthermore, voxels whose density values are in the interval defined by  $c_{lower}$  and  $c_{upper}$  are considered optimal, that means voxels in this area have high probability that they belong to the vessel tissue. The function  $f_I(y)$  is described graphically in Figure 1 and is defined as:

$$f_I(y) = \begin{cases} \infty & f(y) < c_{lowerBorder} \\ (c_{lower} - f(y)) \cdot \omega_{lower} & c_{lowerBorder} \leq f(y) < c_{lower} \\ 0 & c_{lower} \leq f(y) \leq c_{upper} \\ (f(y) - c_{upper}) \cdot \omega_{upper} & c_{upper} < f(y) \leq c_{upperBorder} \\ \infty & c_{upperBorder} < f(y) \end{cases} \quad (2)$$

The function  $f_G(x, y)$  is defined under the assumption that the gradient magnitude is lower in the direction of the vessel center than in the direction of the vessel boundary, and is defined as:

$$f_G(x, y) = |f(x) - f(y)| \quad (3)$$

Finally, the function  $f_L(y)$  is the Laplacian filter and is

used to prevent the algorithm from entering bone structure. Values resulting from the convolution with the Laplace edge detection operator above  $c_{Laplace}$  are considered bone tissue, in the other case are considered to be vessels. More details about the use of this function is given in [KWF\*01].

$$f_L(y) = \begin{cases} \infty & (L \otimes f(y)) > c_{Laplace} \\ 0 & \text{else} \end{cases} \quad (4)$$

The vessel centerline is defined as a 3D curve smoothed by B-Spline technique. The initial path generated by the vessel tracking is taken as the initial approximation of the central axis. Along this path, a perpendicular cross-section is estimated for each point. Each center approximation technique that we present in the following sections is applied to each perpendicular cross-section.

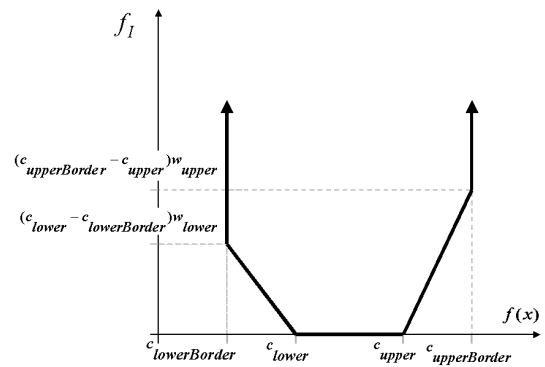


Figure 1: Density interval function from ([KWF\*01]).

### 2.1. Ray Casting

The ray casting method works by tracing several rays from one point inside the object to outside. The idea is to trace several rays  $\vec{r}$  from one initial point inside the object until a boundary is detected, as we can see in Figure 2. Wink et al. [WNV00] and Kanitsar et al. [KWF\*01] use this technique to approximate the vessel centerline.

This technique is applied on a 2D plane. Therefore, the first step is to approximate a perpendicular cross-section along the initial path. For each cross-section with an initial point inside the vessel the new center of the vessel is estimated.

Wink et al. [WNV00], use the gradient information to detect the border of the vessel. First, they calculate the gradient as a convolution of the original image with a normalized Gaussian derivative, in order to reduce noise and other irregularities in the image. Then they define a border as the position where the gradient magnitude, in the direction of the ray, reaches a first maximum above some threshold. The threshold has to be significantly higher than the typical noise level in the data set. This threshold depends on the image quality (e.g., contrast, noise and resolution), and therefore can be modality dependent. On the other hand, Kanitsar et

al. [KWF\*01] apply the ray casting technique based on the density interval function (see Fig. 1) defined above, and stop the ray casted when a density value along the ray is outside this interval. This valid interval for a vessel was defined empirically as:

$$t_{lower} = \frac{c_{lower} - c_{lowerBorder}}{4} + c_{lowerBorder} \quad (5)$$

$$t_{upper} = c_{upperBorder} - \frac{c_{upperBorder} - c_{upper}}{4} \quad (6)$$

For the evaluation we implemented two ray casting techniques. We denote one as ray casting with thresholds (RCT) and the other as ray casting with maximum gradient (RCMG). The RCT is the same ray casting technique used by Kanitsar [KWF\*01]. RCMG uses the maximum gradient along the ray as stopping criterion. For the RCMG method we use the lower threshold value  $t_{lower}$  to be sure we are not taking background information or other tissue with lower density values than the vessels.

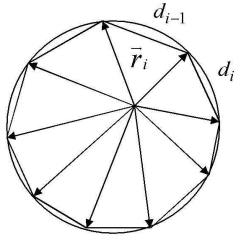


**Figure 2:** Example of the ray casting method

After several border points are estimated, the true center is calculated by:

$$[x_c, y_c] = \left[ \frac{\sum_{i=1}^n x_i (d_{i-1} + d_{(i) \bmod (n)})}{2 \sum_{i=1}^n d_i}, \frac{\sum_{i=1}^n y_i (d_{i-1} + d_{(i) \bmod (n)})}{2 \sum_{i=1}^n d_i} \right] \quad (7)$$

Here,  $x_c$  and  $y_c$  are the coordinates of the center calculated,  $n$  is the number of border points detected,  $x_i$  and  $y_i$  are the coordinates of the  $i$ -th border point, and  $d_i$  is the distance between two adjacent border points  $i$  and  $i+1$ . The function  $\bmod$  is used due to the circular connection between successive border points.

## 2.2. Block Matching

The Block Matching technique is used for motion estimation between successive frames in video compression [HSHK00]. More details about this technique are described in [DKF95]. In essence this method tries to look for the best matching between two images by applying a shift on the original images. This method is based on the assumption that two consecutive images  $f_{2D}(x, y, 0)$  and  $f_{2D}(x, y, 1)$  are related by a simple shift, where  $f_{2D}(x, y, k)$  is the density value of the 2D image at time  $k$ . Davis et al. [DKF95] relates two images as:

$$f_{2D}(x, y, 1) = f_{2D}(x - x_d, y - y_d, 0), \quad (8)$$

where  $x_d$  and  $y_d$  represent the displacement of the image from time 0 to time 1. These values are estimated by minimizing the magnitude of the difference between shifted states of the two images as:

$$(\hat{x}_d, \hat{y}_d) = \min_{x'_d, y'_d} \sum_{i,j} [f_{2D}(i + x'_d, j + y'_d, 1) - f_{2D}(i, j, 0)]^2, \quad (9)$$

where the displacements  $x'_d$  and  $y'_d$  are integer multiples of pixels in the image space.

## 2.3. Center Of Gravity

The weighted center of gravity has been used widely in order to estimate the object center with sub-pixel precision [vAEPR02]. The center of gravity can be defined as the equilibrium point where the entire weight of the object is concentrated. For a 2D gray level image the center of gravity is defined in [vAEPR02] as:

$$[x_c, y_c] = \left( \frac{\sum_{x,y \in \Omega} x w(x, y)}{\sum_{x,y \in \Omega} w(x, y)}, \frac{\sum_{x,y \in \Omega} y w(x, y)}{\sum_{x,y \in \Omega} w(x, y)} \right), \quad (10)$$

where  $\Omega$  defines the area containing pixels that belong to the vessel, and  $w(x, y)$  the weighted function for each coordinate in the  $\Omega$  space, and is defined as:

$$w(x, y) = a(f_{2D}(x, y) - m) \quad (11)$$

and,

$$m = \min_{x,y \in \Omega} (f_{2D}(x, y)) \text{ when } a > 0 \text{ or} \quad (12)$$

$$m = \max_{x,y \in \Omega} (f_{2D}(x, y)) \text{ when } a < 0 \quad (13)$$

For  $a > 0$  the center of gravity is attracted to the center of brighter pixels (high intensity) of the object, and for  $a < 0$  darker pixels. In our case, we are interested in brighter pixels, therefore we used  $a = 1$ . Assuming that in the center of the vessel we have higher intensity value for vessel pixels. The function  $f_{2D}(x, y)$  corresponds to density value of a pixel  $(x, y)$  in the 2D perpendicular cross-section.

Assen et al. [vAEPR02] present an analysis of the accuracy and precision of object localization in gray level images using the center of gravity. Furthermore, they analyzed the influence of applying a threshold for a possible accuracy and precision of the center of gravity measure. They conclude that in order to find a best estimate for the center of gravity in a gray level image a threshold should be applied. In this way, we used the threshold values  $t_{lower}$  and  $t_{upper}$  defined in Eq. 5 and 6 respectively, to estimate the center of gravity of points with high probability that they belong to vessel tissues.

## 2.4. Ellipse Fitting

Blood vessels have a tubular structure, which could be defined by a set of elliptical shapes along its axis. Therefore, an approximation to the centerline of the vessel should be by defining an elliptical parametrization along its axis. Starting

from the initial path obtained from the vessel tracking, the Canny edge detector [Can86] is applied in order to get a set of points around the vessel boundary. Then, these points are approximated with an ellipse using the Lagrange multiplier technique. Fitzgibbon et al. [FF95] present a system solution used to extract a conic section from image data in order to estimate a center and radii of circles or ellipses from a set of points. Fitzgibbon describes the problem as:

Given:

- A set of 2D Points  $P = \{\mathbf{x}_i\}_{i=1}^n$ , where  $\mathbf{x}_i = (x_i, y_i)$
- A curve  $C(\mathbf{a})$  parameterized by the vector  $\mathbf{a}$
- A distance metric  $\delta(C(\mathbf{a}), \mathbf{x})$  as a measure of the distance from a point  $\mathbf{x}$  to the curve  $C(\mathbf{a})$

The method consists of finding the  $\mathbf{a}_{min}$  for which the error function  $error = \sum_{i=1}^n \delta(C(\mathbf{a}), \mathbf{x}_i)$  reaches a global minimum. An implicit representation of a curve is  $C(\mathbf{a}) = \{\mathbf{x} | F(\mathbf{a}, \mathbf{x}) = 0\}$ , in our case  $F(\mathbf{a}, \mathbf{x})$  is the representation of general conic curves which is given by:

$$F(\mathbf{a}, \mathbf{x}) = ax_i^2 + bx_iy_i + cy_i^2 + dx_i + ey_i + f = \begin{bmatrix} x_i^2, x_iy_i, y_i^2, x_i, y_i, 1 \end{bmatrix} [a, b, c, d, e, f]^T, \quad (14)$$

where  $\mathbf{a} = [a, b, c, d, e, f]^T$ , and  $\mathbf{x} = [x_i^2, x_iy_i, y_i^2, x_i, y_i, 1]^T$ . Eq. 14 is called the algebraic distance. The problem consists on minimizing the sum of squared algebraic distances  $\sum_{j=1}^n F(\mathbf{a}, \mathbf{x})^2$  with the constraint that for an ellipse  $4ac - b^2 = 1$ . After, this optimization problem is solve [FF95], the ellipse center and axis can be extracted from the equation.

## 2.5. Randomized Hough Transform

The Hough Transform (HT) is a technique for detecting parametric curves of a given shape in an image. First, all the points of interest that involve the object or the shape of interest have to be extracted. These points can be extracted using some edge detector method. Now, we have a set of points which is our input data. Second, a parametric space has to be defined, this parametric space consist of a cell, which represents a set of parameter of a parametric curve of interest. We are interesting in extract elliptical shapes and an ellipse can be defined by 5 parameters  $(a, b, x_c, y_c, \alpha)$ . Here,  $a$  and  $b$  correspond with the major and minor radii of the ellipse respectively,  $x_c$  and  $y_c$  the center and  $\alpha$ , the angle of rotation. This parameter space is used as an histogram. In our case, for each ellipse found in the input data a cell corresponding with the parameters of the ellipse founded is incremented by one. After all possible ellipse is extracted, peaks in the histogram represent a possible ellipse that we can extract from the image. The RHT technique which is an extension of HT [XOK90], consists of randomly selecting a subset of points that approximate a curve. The process is repeated until a certain number of times, defined previously.

In our case, we use the Canny edge detector method

[Can86], in order to extract the set of points of interest (input data). Then, parametric ellipses are extracted using the technique defined by McLaughlin [Mac98]. He describes an accurate method to improve the ellipse detection in an image using the RHT. This technique consists of randomly selecting three points ( $P_1$ ,  $P_2$ , and  $P_3$ ) from the input data, and defining the ellipse that passes through these points (see Figure 3). For each point  $P_i$  the tangent to the curve is estimated, selecting a neighborhood around this point and finding by least square, the line of best fit to the curve in this neighborhood. The mid point  $m$  between  $P_1$  and  $P_2$  is calculated, and intersected with the intersection point  $t$  between the tangents of these points (see Figure 3(a)). The possible center of the ellipse will lie in the line defined by  $tm$ . The process is repeated with the points  $P_2$  and  $P_3$ , which define a second line. The intersection of these two lines will be the center of the ellipse.

With the center of the ellipse detected  $c$  (see Figure 3(b)) whose coordinates are  $(x_c, y_c)$ , and the three points  $P_1 = (x_1, y_1)$ ,  $P_2 = (x_2, y_2)$ , and  $P_3 = (x_3, y_3)$  a possible ellipse is estimated as:

- The ellipse equation (derived from Eq. 14 [Wei98]) is defined as:

$$a(x - x_c)^2 + 2b(x - x_c)(y - y_c) + c(y - y_c)^2 = 1 \quad (15)$$

With the restriction  $(ac - b^2) > 0$

- Translating the center to the origin, equation 15 is reduced to:

$$ax^2 + 2bxy + cy^2 = 1 \quad (16)$$

- If the coordinates from  $P_1$ ,  $P_2$ , and  $P_3$  are substituted in equation 16 we have the following equation system:

$$\begin{bmatrix} x_1^2 & 2x_1y_1 & y_1^2 \\ x_2^2 & 2x_2y_2 & y_2^2 \\ x_3^2 & 2x_3y_3 & y_3^2 \end{bmatrix} \begin{bmatrix} a \\ b \\ c \end{bmatrix} = \begin{bmatrix} 1 \\ 1 \\ 1 \end{bmatrix} \quad (17)$$

- After solving the equation system from 17 we get the parameters  $(x_c, y_c, a, b, c)$ .
- The parameter  $(x_c, y_c, a, b, c)$  must be converted into polar coordinates [Wei98]  $(x_c, y_c, r_1, r_2, \theta)$ , where  $r_1$  and  $r_2$  are the radii of the major and minor axis respectively of the ellipse, and  $\theta$  is the angle of rotation for the major axis. In this way we get the parameter of the ellipse.

Then, we must validate that the possible ellipse found exist in the data. This process is done, drawing the ellipse in the image and look for all the possible points that exist in the data image and it is part of the border of this ellipse. For each ellipse found in the input data, it must be validated, more details in [Mac96]. For each valid ellipse detected, a 5-D accumulator is used to count the number of valid ellipses found. After a predefined number of iterations, the cell with the maximum value in the 5-D accumulator determines the parameters for the best ellipse found in the image.

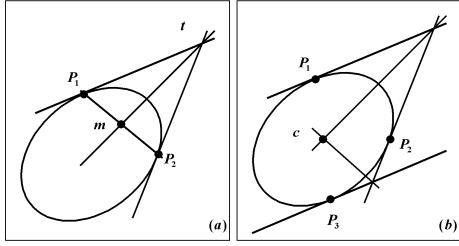


**Figure 3: Ellipse Approximation.** (a) Estimation of line where the ellipse center should pass. (b) Estimation of the ellipse center.

### 3. Evaluation

Three different synthetic data sets have been used to evaluate the accuracy of each method. Each synthetic data set consists of 3D data of  $256 \times 256 \times 768$ , and it simulates a vessel structure of peripheral arterial tree, from aorta-to-pedal. The vessel diameter varies along the z-axis from about 0.7 to about 23 voxels, from the slice 768 to the slice 0. The density for a vessel is defined between 1130 and 1350 and the background density between 1080 and 1100. The curvature of the data is defined by a helix with an angle of 32.14 and radius 76.8. Each data set presents some Gaussian noise, which are added with sigma 0, 5 and 10 respectively. An example of the synthetic data is shown in figure 4.



**Figure 4: MIP of the synthetic data.**

In the following, we present the results of several experiments. First, for the evaluation of the centerline estimation a graph was generated and it describes the error of the distance between the center in the synthetic data, which is known, and the center estimated by the method. The RCT, RCMG, EF and RHT methods estimate the vessel centerline and its diameter in each slices, while the CoG and BM estimate just the vessel centerline. For this reason, we generate two kind of graphs, the first shows the distance error and the second shows graphically how far is the real diameter of the vessel

from the diameter estimated. Both graphs are plotted along the vessel.

The RCT technique uses two threshold values  $t_{lower}$  and  $t_{upper}$ . These two values define a valid interval to identify vessels. For the evaluation we change this interval. We start using  $t_{lower}$  and  $t_{upper}$  as we show in Eq. 5 and 6. The result is presented in Figure 5(a) and 5(b). After several experiments where this interval was defined wider and wider until reach  $t_{lower} = c_{lowerBorder}$  and  $t_{upper} = c_{lowerUpper}$ , we observed better results (see Figure 5(c) and 5(d)). The irregularity presented between slice 500 and 600 is due to this area the synthetic data set presents some noise getting dark the intensity of the vessel. Nevertheless, if we modify the threshold values we can get better results as we can see in Figures 5(c) and 5(d). For The RCMG technique we use the lower threshold  $t_{lower}$  used by RCT in order to be sure we are not taking pixel whose intensity values belong to background. We did the same experiment as we did for the RCT technique. The results are shown in Figure 6. Between these two methods the RCT show better results than RCMG using our synthetic data set. The BM method uses a reference image to make matching, which is initially centered. This reference image is taken from the previous results obtained with the last block matching estimation. As experiment, initially we fix the mask and make the matching process with the successive slices until reach 5 slices or 10 slices, where we update the mask with the new matching result. These numbers (5 and 10) were selected empirically, as experiment. In Figures 7(b), 7(c) we can see the results updating the mask each 5 and 10 slices respectively. This method has to be improved to get better results, using an optimization process in the search of the best matching point and using subpixel precision. For the CoG we did two experiments. As first experiment, we set the weighted function  $w(x,y) = 1$  (see Eq. 10). For the second experiment we set  $w(x,y)$  as we defined in Eq 11. The CoG technique uses the two threshold values to identify the vessel. We modify this interval in the same way as we did for RCT method. As we can see in Figure 8. These results tell us that this method is also threshold depending like RCT. EF uses as preprocessing step an edge detector technique, in our case we use the Canny edge detector [Can86]. The Canny method uses two threshold values. These threshold values can be defined base on the density function for a vesel. After several experiments modifying theses thresholds used for preprocessing, we can show the best result we get (see Figure 9). The RHT fails many times especially in small diameters due to there are not enough points in this area to find an ellipse. In Figure 10(a) and 10(b) we can see the results.

Respect with the time consume for each method we present the table 1, here we observe that BM has the high time consume than the others method. And RCT, RCMG and CoG keep the time in the same rank of value, there is not significative difference. Meanwhile, EF increment a bit the time but still is tolerable.

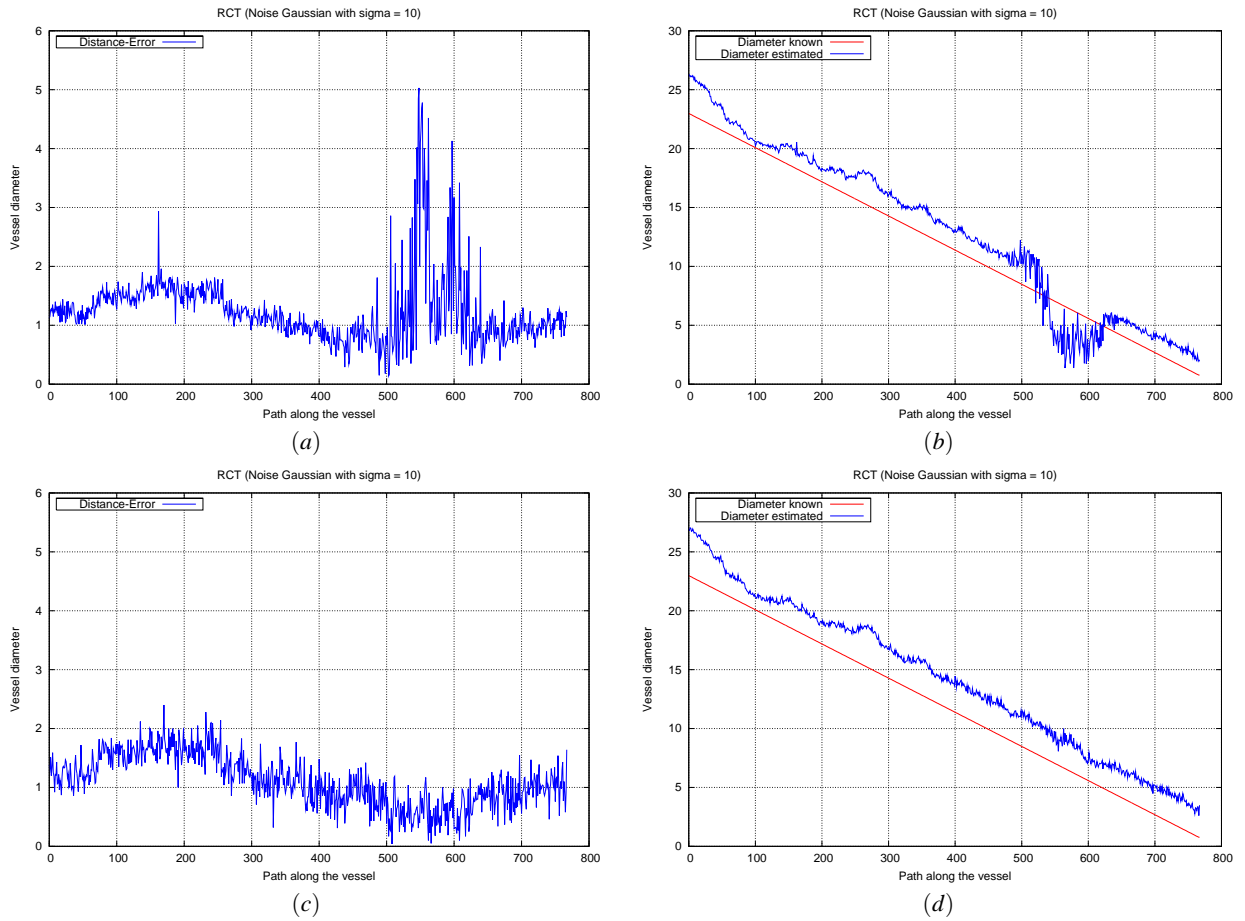


**Figure 5:** Result from RCT technique. (a) and (c) Distance error of the center estimated. (b) and (d) Diameter estimated. In (a) and (b) we used threshold values defined with Eq. 5 and 6. Finally, in (c) and (d) we use  $t_{lower} = c_{lowerBorder}$  and  $t_{upper} = c_{upperBorder}$ .

RCT	RCMG	EF	CoG	BM	RHT
1.797	1.594	3.969	1.531	174,000	104,000
1.703	1.625	3.703	1.515	198,000	100,000
1.703	1.859	3.750	1.531	173,000	101,000

**Table 1:** Time consume for each method in seconds.

#### 4. Conclusion

The paper presented an evaluation of different techniques used to approximate the center of the vessel in the peripheral arterial tree. We used a synthetic data in order to evaluate the accuracy of each method. In general all methods are sensible to noise, nevertheless the CoG method present less

sensibility to noise than the others. RCT, RCMG and CoG methods present the best approximation to the center. BM can be optimized, in order to improve the performance and accuracy, using sub-pixel motion precision and optimizing the searching process. We are afraid with The RHT in small diameter there is not enough points. In this work we use the same method from MacLaughlin [Mac96] to implement the RHT, we found many parameters and threshold values we must handle in a precise way. This make difficult an accuracy evaluation of this method for small diameters. The RCT technique uses two threshold values,  $t_{lower}$  and  $t_{upper}$ . These values were selected empirically from the density function described in Figure 1. Higher values for this interval result on erroneous estimation of the center due to the inclusion of pixels whose density values belong to other tissues. Lower values for this interval do not allow us to find vessel voxels. The RCMG technique uses the lower threshold value

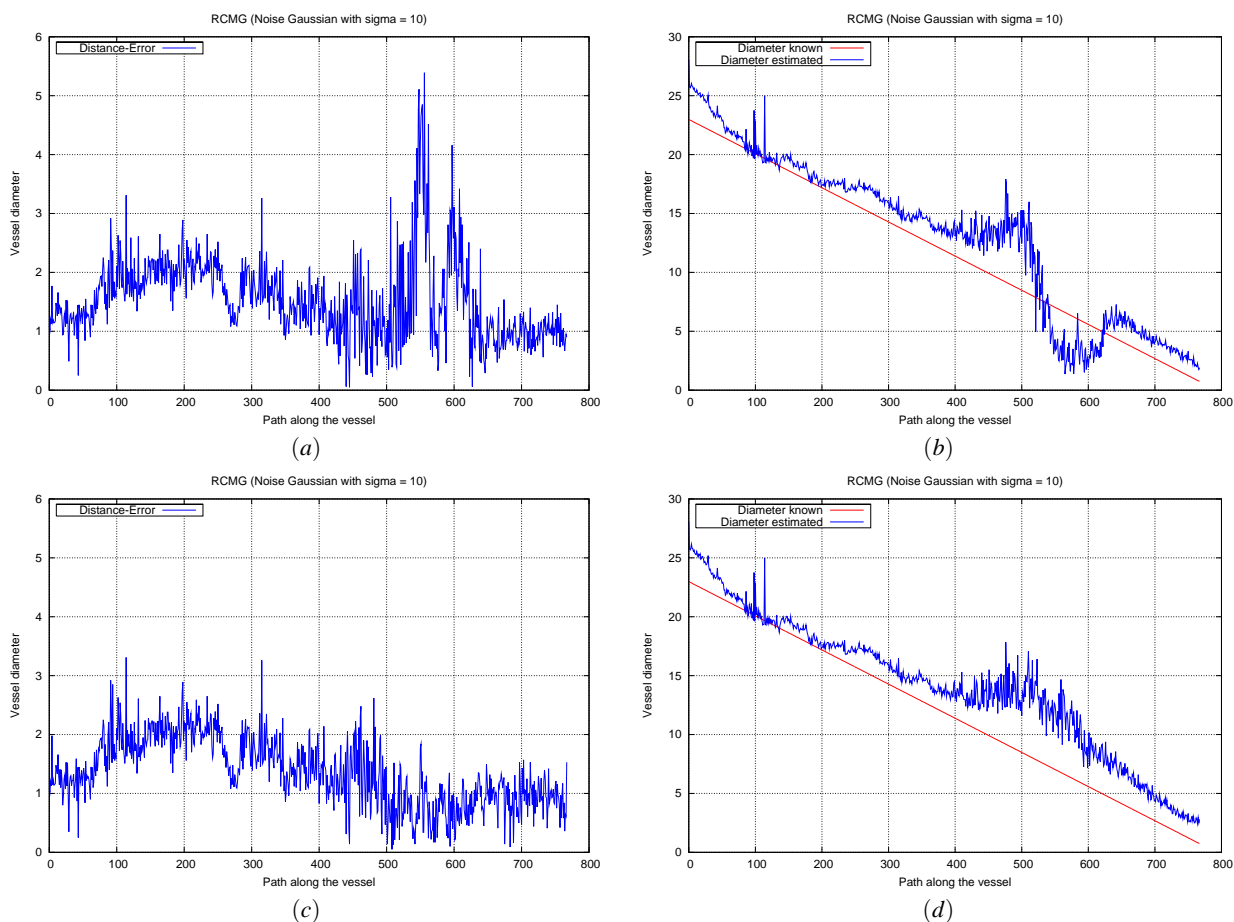


**Figure 6:** Result from RCMG technique. (a) and (c) correspond with the distance error of the centerline and (b) and (d) the diameter estimation. In (a) and (b) we used lower threshold defined with Eq. 5, in (c) and (d)  $t_{lower} = c_{lowerBorder}$ .

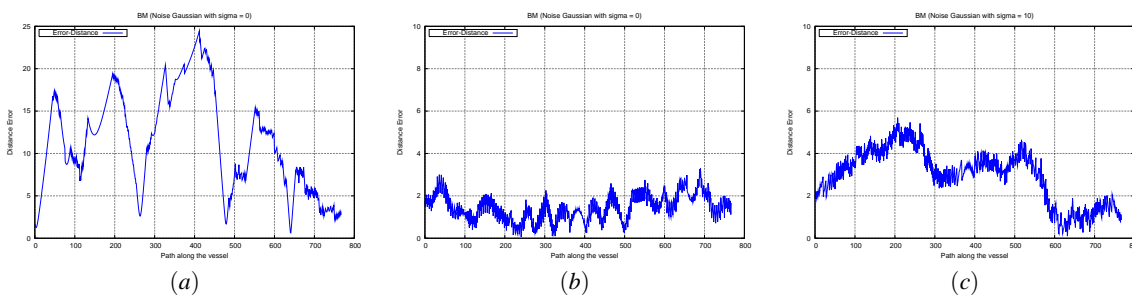


**Figure 7:** Results from Block Matching technique. (a) Slice by slice (b) updating the image reference each 5 Slices (c) each 10 slices.

$t_{lower}$  from RCT. In real data, if the vessel is far from bone structure, it shows better results than the RCT technique, especially on calcified vessels (see Figure 11 first and second

row)). In Figure 11 (First row, second column) we can observe a pseudoestenosis due to a bad approximation of the center, while in Figure 11 (Second row, second column) the

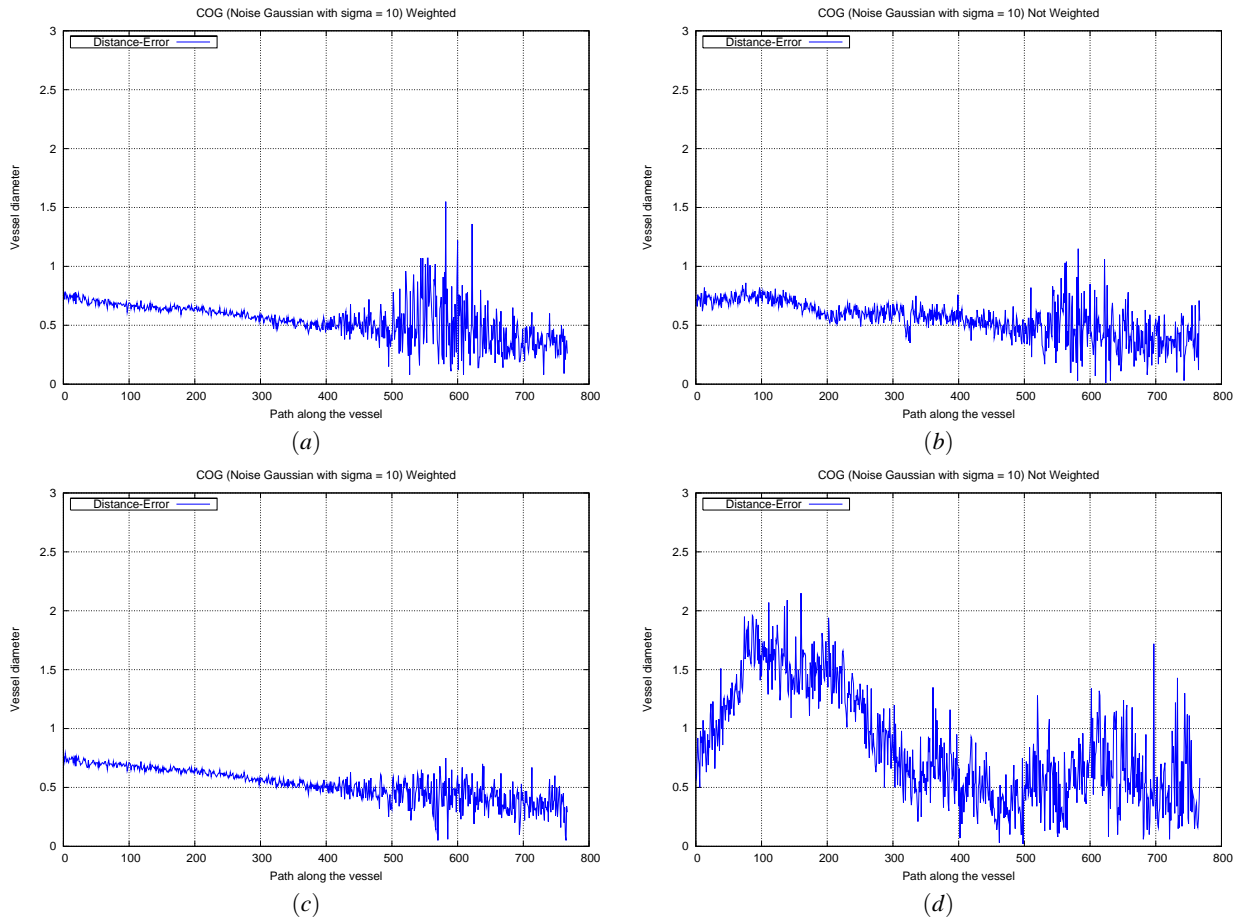


**Figure 8:** Results from CoG technique. Figures (a) and (b) show the distance error of the centerline and the diameter estimation respectively, in this case we use thresholds defined in Eq. 5 and 6. (c) and (d) use as thresholds  $t_{lower} = c_{lowerBorder}$  and  $t_{upper} = c_{upperBorder}$ .

RCMG make a better approximation of the center. The BM technique requires an optimization process for better results. Initially we assume that between successive cross-sections the images are related by a simple shift. If we define an interval to update the mask used like reference image for the matching process, this method show better results. The CoG technique has two parameters:  $t_{lower}$  and  $t_{upper}$ , which are threshold values to classify pixels that belong to the vessel. Small threshold interval implies that few pixels are computed and large threshold interval includes more pixels whose density value could belong to other tissues. The EF technique depends on the parameters of the Canny edge detector. The Canny edge detector uses two thresholds values for the "hysteresis process" involved in the method, which classify the pixels resulting from a previous Gaussian filtering, gradient and non-maximum suppression steps [Can86]. As Fitzgibbon [FF95] mentions in his work, this method ex-

hibits some problems if the data do not correspond very well to the contour. This occurs if we do not get a good estimation of the vessel boundary with the Canny edge detector method. The RHT technique depends also on the parameters of the Canny edge detector, and is computationally expensive, and for small diameters result quite difficult extract by least square the tangent of a curve defined in one of the randomly point selected. There is not enough point for small diameters of the object. In general, all methods are sensible to noise. The CoG technique presented better results even under noise influence. RCT and RCMG shows quite similar results.

## References

- [BFC03] BÜHLER K., FELKEL P., CRUZ A. L.: Geometric methods for vessel visualization and

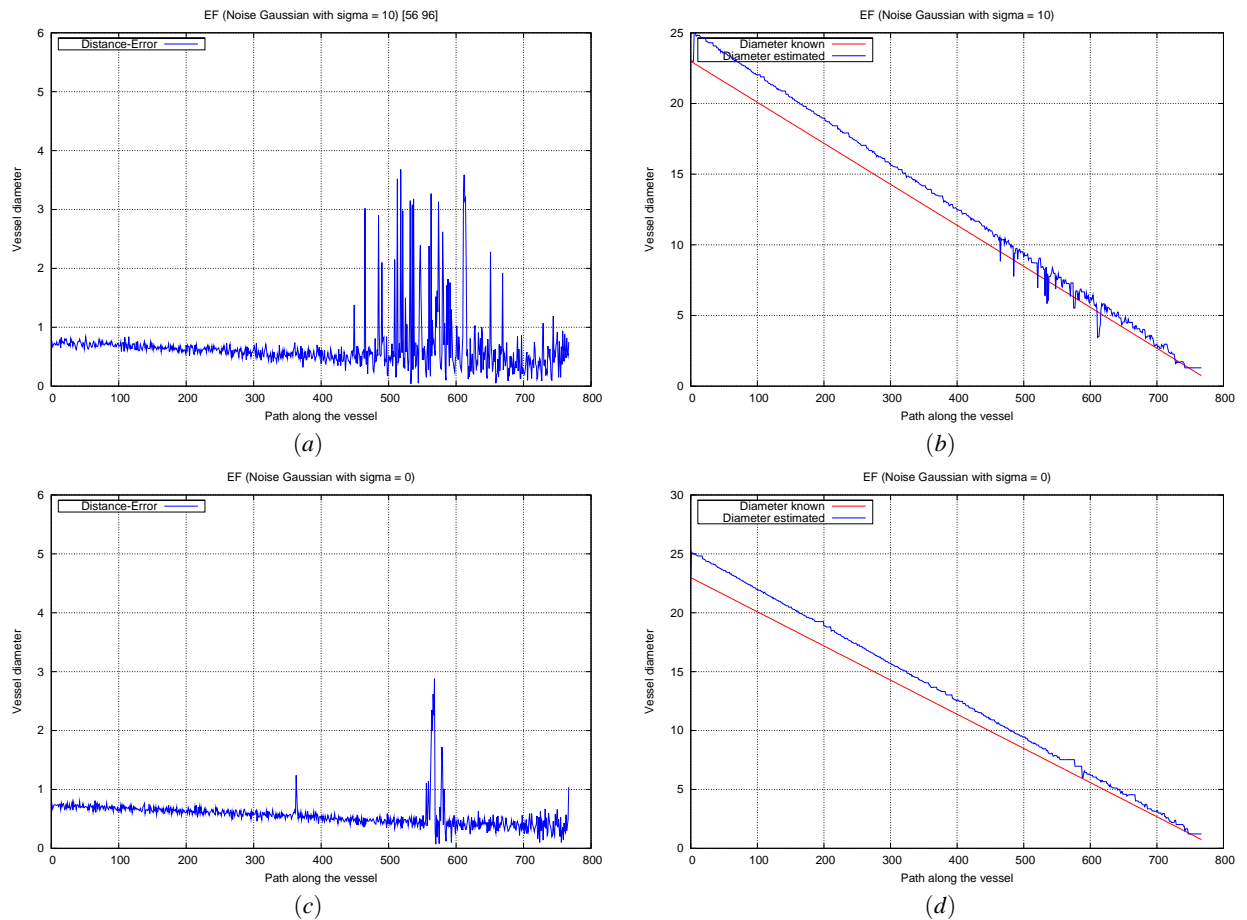


**Figure 9:** Results from EF technique. (a) and (b) correspond with the distance error of the centerline and the diameter estimated, with a noise data with  $\sigma = 10$  and (c) and (d) without noise.

- quantification - a survey. In *Geometric Modelling for Scientific Visualization* (2003), G. Brunnet, B. Hamann and H. Müller (eds.). Kluwer Academic Publishers.
- [Can86] CANNY J.: A computational approach to edge detection. *IEEE Trans. Pattern Anal. Mach. Intell.* 8, 6 (1986), 679–698.
- [CRC92] COATRIEUX J. L., RONG J., COLLAREC R.: A framework for automatic analysis of the dynamic behavior of coronary angiograms. *Int. J. Cardiac Imag.* 8 (1992), 1–10.
- [Dij59] DIJKSTRA E. W.: A note on two problems in connection with graphs. *Numerische Mathematik* (1959), 269–271.
- [DKF95] DAVIS C. Q., KARU Z. Z., FREEMAN D. M.: Equivalence of subpixel motion estimators based on optical flow and block matching. In *International Symposium on Computer Vision* (1995), pp. 7–12.
- [FF95] FITZGIBBON A., FISHER R.: A buyer's guide to conic fitting. In *British Machine Vision Conference* (1995), pp. 513–522.
- [HSHK00] HWANG-SEOK O., HEUNG-KYU L.: Block-matching algorithm based on an adaptive reduction of the search area for motion estimation. *Real Time Imaging* 6 (2000), 407–414.
- [KFW\*02] KANITSAR A., FLEISCHMANN D., WEGENKITTL R., FELKEL P., GRÖLLER M. E.: CPR - Curved Planar Reformation. In *IEEE Visualization 2002* (Oct. 2002), pp. 37–44.
- [KQ00] KIRBAS C., QUEK F.: *A Review of Vessel Extraction Techniques and Algorithms*. Tech.

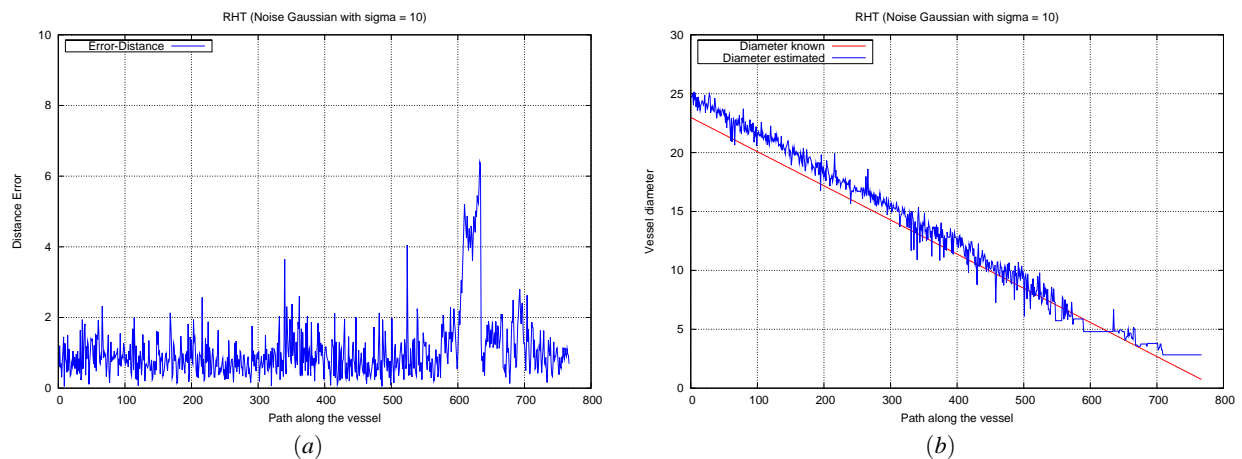


**Figure 10:** Result from RHT technique. (a) correspond with the distance error of the centerline and (d) the diameter estimated

- rep., VisLab Wright State University, Dayton, Ohio, Nov 2000.
- [KTS88] KITAMURA K., TOBIS J., SKLANSKY J.: Estimating the 3d skeletons and transverse areas of coronary arteries from biplane angiograms. *IEEE Transaction Medical Images 7* (1988), 173–187.
- [KWF\*01] KANITSAR A., WEGENKITTL R., FELKEL P., FLEISCHMANN D., SANDNER D., GRÖLLER E.: Computed tomography angiography: a case study of peripheral vessel investigation. In *Visualization* (2001), IEEE, pp. 477–480.
- [Mac96] MACLAUGHLIN R. A.: Randomized hough transform: Better ellipse detection. In *IEEE TENCON. Digital Signal Processing Applications* (1996), IEEE, pp. 409–414.
- [Mac98] MACLAUGHLIN R. A.: Randomized hough transform: Improved ellipse detection with comparison. In *Pattern Recognition Letters 19* (1998), pp. 299–305.
- [NKSK93] NIKI N., KAWATA Y., SATO H., KUMAZAKI T.: 3d imaging of blood vessels using x-ray rotational angiographic system. In *Medical Imaging Conference* (1993), IEEE, pp. 1873–1877.
- [PGJ03] PAREDOS P., GOLOB M., JENSTERLE M.: Interrelationship between peripheral arterial occlusive disease, carotid atherosclerosis and flow mediated dilation of the brachial artery. *International Angiology* (March 2003), 22(1):83-7.
- [PTN97] PUIG A., TOST D., NAVAZO I.: An interactive cerebral blood vessel exploration system. In *IEEE Visualization '97* (1997), Yagel R., Hagen H., (Eds.), IEEE, pp. 443–446.
- [Pui98a] PUIG A. P.: *Cerebral Blood Vessels Modelling*. Tech. Rep. LSI-98-21-R, Universitat Politècnica de Catalunya, 1998.
- [Pui98b] PUIG A. P.: *Discrete Medial Axis Transform for Discrete Objects*. Tech. Rep. LSI-98-22-R, Universitat Politècnica de Catalunya, 1998.
- [TKN\*95] TOZAKI T., KAWATA Y., NIKI N., OHMATSU H., MORIYAMA N.: An approach for detecting blood vessel diseases from cone-beam ct image. In *IEEE Nuclear Science Symposium and Medical Imaging Conference* (1995), IEEE, pp. 1470–1474.
- [vAEPR02] VAN ASSEN H., EGMONT-PETERSEN M., REIBER J.: Accurate object localization in gray level images using the center of gravity measure; accuracy versus precision. *IEEE Transactions on Image Processing 11, 12* (December 2002), 1379–1384.
- [Wei98] WEISSTEIN E.: *CRC Concise Encyclopedia of Mathematics*. Boca Raton, FL: CRC Press, 1998.
- [WNV00] WINK O., NIESSEN W., VIERGEVER M.: Fast delineation and visualization in 3-d angiographic images. *IEEE Transactions on Medical Imaging* (2000).
- [XOK90] XU L., OJA E., KULTANEN P.: A new curve detection method: Randomized hough transform (rht). In *Pattern recognition Letters* (1990), pp. 331–338.

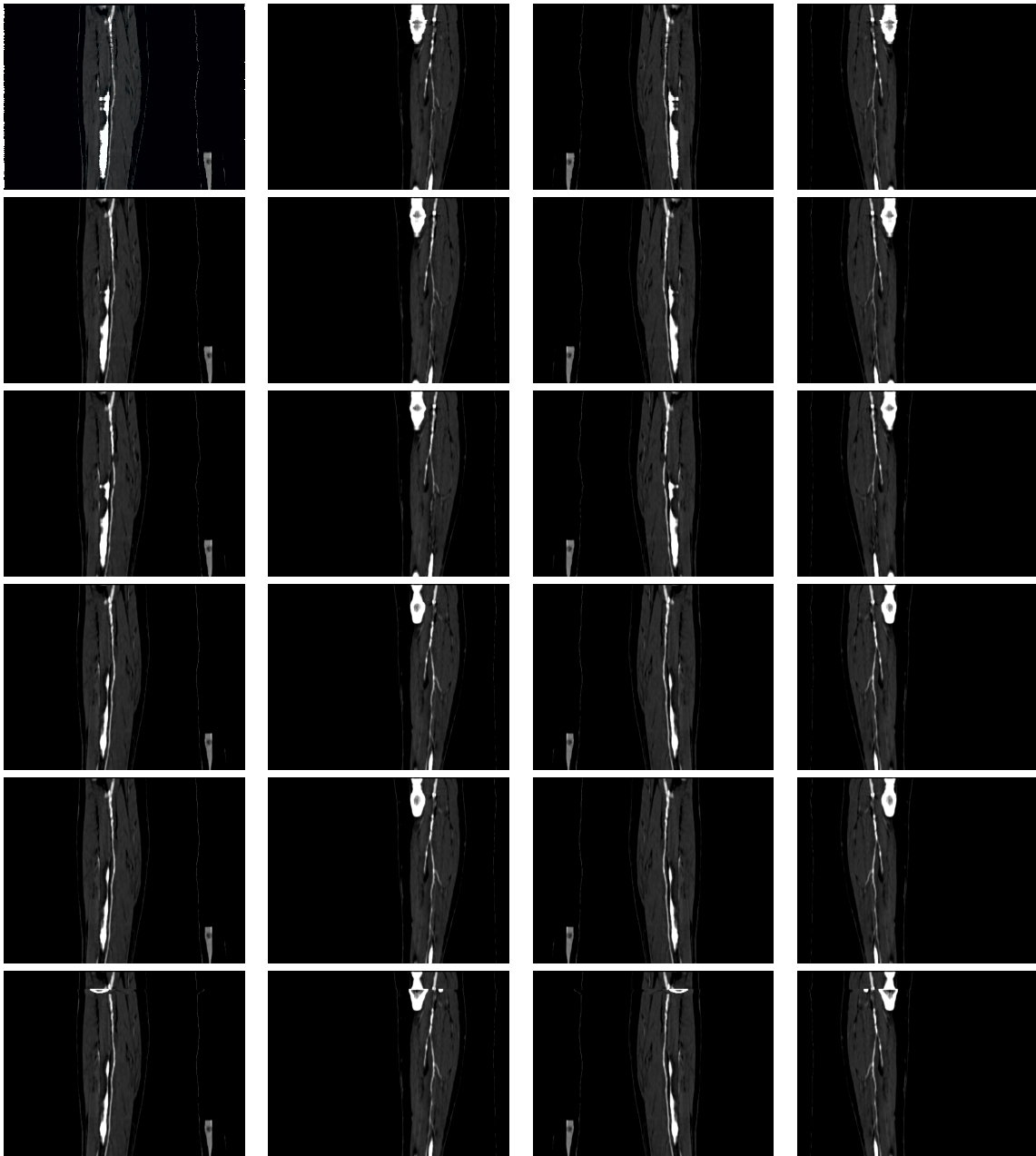


**Figure 11:** From left to right rotating CPR with 45, 135, 225 and 315 degree. From top to bottom Centered with RCT, RCMG, CoG, EF, BM and RHT. This data correspond to a femoral with a diameter between 2mm and 4mm. Brighter objects correspond to bone structures, in some images appear closer to the vessel.